High-Speed Interrogation System for Fiber Bragg Gratings With Buffered Fourier Domain Mode-Locked Laser

Tatsuya Yamaguchi, *Member, IEEE*, Wataru Endo, *Member, IEEE*, and Yukitaka Shinoda, *Member, IEEE*

***Abstract*—We develop a high-speed interrogation system with a wavelength-swept laser for sensing multiplexed fiber Bragg gratings (FBGs). High-speed and multipoint sensing is achieved by means of a buffered Fourier domain mode-locked (FDML) laser, a recently proposed high-speed wavelength-swept laser. This laser increases the measurement rate several times by tailoring the laser output with a buffer stage. The developed buffered FDML laser successfully achieves a measurement rate of 202.8 kHz using a general FDML laser driven at a sweep rate of 50.7 kHz. In order to detect reflection signals of FBGs at the high measurement rate, the measurement system introduces digital signal processing using a field programmable gate array (FPGA). However, FBG measurements with wavelength-swept lasers are affected by the propagation time (delay) in the optical fiber connecting from the laser to the FBG sensor, which reduces measurement accuracy. To overcome this limitation, the developed system uses a delay correction method with bidirectional sweep of the buffered FDML laser. The interrogation system with the buffered FDML laser achieves a time resolution of 4.9 μs without being affected by the delay.**

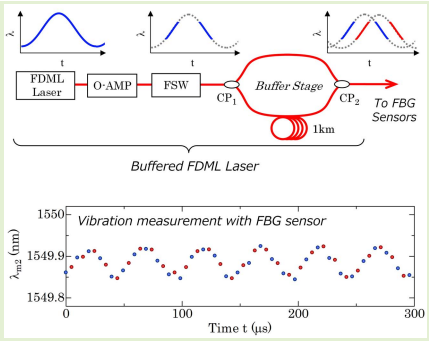

***Index Terms*—Optical fiber sensors, fiber lasers, sensor systems, real-time systems.**

I. Introduction

HIGH-SPEED wavelength-swept lasers are key optical sources in many fields of science and engineering. In biomedical optics, high-speed wavelength-swept lasers have dramatically improved optical coherence tomography (OCT) imaging speeds and detection sensitivities for biological tissues [1]. The Fourier domain mode-locked (FDML) laser has recently been studied as a novel type of high-speed wavelength-swept laser [2]. The FDML provides high sweep rates exceeding several tens of kHz, which enables it to be used as an optical source for the fastest OCT systems. Owing to their excellent performance, there has been considerable interest in the use of FDML lasers in various applications such as compressed pulse generation [3], optical absorption spectroscopy [4], and optical fiber sensing [5]–[8].

Several studies have focused on measurements of fiber Bragg grating (FBG) sensors by introducing FDML lasers [5]–[8]. Various optical fiber-sensing methods, such as through the use of interferometers, optical combs, spectroscopy, and laser modulation, have been proposed to improve the measurement performance [9]–[20]. FBGs, well-known as optical fiber-type sensors of strain and vibration, have several key advantages owing to their high sensitivity, insensitive to electromagnetic interference, and fast response [21]–[24]. Sensor multiplexing can be achieved by serially arranging FBGs with different Bragg wavelengths on a single optical fiber. In general measurements using wavelength-swept lasers, the emission wavelength is repeatedly swept over the spectra of FBGs [25]–[27]. Wavelength information is encoded as time information in FBGs, and measurement rates are limited to the sweep rates of wavelength-swept lasers. Therefore, using FDML lasers with high sweep rates for measurements could potentially enable novel types of FBG interrogation systems capable of multipoint sensing above several tens of kHz. Although high-speed measurements of FBGs have

Manuscript received April 13, 2021; accepted May 2, 2021. Date of publication May 11, 2021; date of current version July 30, 2021. This work was supported in part by the Grant-in-Aid for Early-Career Scientists under Grant 20K14754 and in part by the College of Science and Technology Project for Research, Nihon University. The associate editor coordinating the review of this article and approving it for publication was Dr. Anuj K. Sharma. *(Corresponding author: Tatsuya Yamaguchi.)*

Tatsuya Yamaguchi and Yukitaka Shinoda are with the Department of Electrical Engineering, College of Science and Technology, Nihon University, Tokyo 1010062, Japan (e-mail: yamaguchi.tatsuya@nihon-u.ac.jp; shinoda.yukitaka@nihon-u.ac.jp).

Wataru Endo is with the Department of Electrical Engineering, Graduate School of Science and Technology, Nihon University, Tokyo 1010062, Japan (e-mail: cswa19008@g.nihon-u.ac.jp).

Digital Object Identifier 10.1109/JSEN.2021.3079191

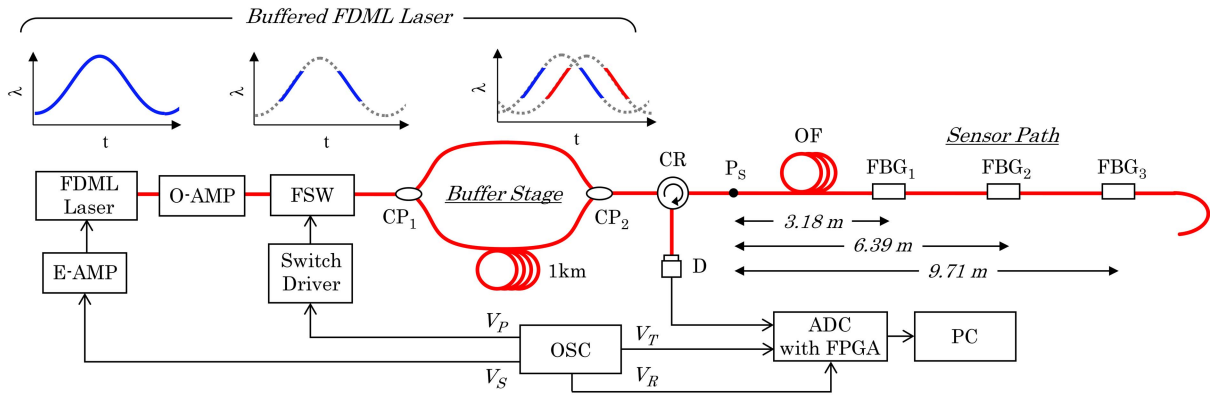

Fig. 1. FBG interrogation system with buffered FDML laser. O-AMP: optical amplifier; FSW: fiber switch; CP: coupler; CR: circulator; Ps: reference position; OF: offset fiber; D: detector; E-AMP: electrical amplifier; OSC: oscillator; ADC: analog-digital converter; FPGA: field programmable gate array; V_P: pulse control signal; V_S: sweep control signal; V_T: trigger signal; V_R: reference clock signal.

been widely demonstrated in previous studies [5]–[8], few studies have focused on signal processing systems for real-time measurements. Thus, we developed a real-time interrogation system based on a field-programmable gate array (FPGA) for high-speed digital signal processing [28]–[30].

However, interrogation systems using high-speed wavelength-swept lasers have lower measurement accuracy owing to the propagation time (delay) in the optical fiber. To solve this problem, delay correction methods using a frequency comb or a Fabry–Perot etalon have been proposed [31], [32]. Our previous research proposed a method for correcting the delay with a bidirectional sweep of wavelength-swept lasers [28], [30]. To install FBGs at long distances or large intervals, correction methods by modulating the sweep rates of wavelength-swept lasers have been reported [33]. We introduced a delay correction method that used pulse modulation with wavelength-swept lasers to automatically recognize reflection signals from multiple FBGs installed at arbitrary long distances and removed delays [34].

In recent years, various vibration sensors have been widely exploited for sensing applications, including in the health monitoring of composite materials and acoustic imaging [35]–[39]. The desirable characteristics of vibration sensors include fast response, sensor multiplexing, small size, stability, and durability in harsh environments. FBG measurements with wavelength-swept lasers have the potential to satisfy these requirements and to capture acoustic emission waves above hundreds of kilohertz. Therefore, speeding up measurement systems further is desirable. Buffered FDML has been recently reported as a novel technique for multiplying the sweep rates of FDML lasers [40]. Although the acceleration of measurements for OCT has recently been reported in the literature [41], very few studies have reported high-speed measurements of FBGs with buffered FDML lasers. In addition, there are very few reports of interrogation systems that are capable of performing multipoint and real-time measurements exceeding the measurement rate of 200 kHz using wavelength-swept lasers.

In this paper, we propose and develop a high-speed interrogation system based on a buffered FDML laser for sensing FBGs. The buffered FDML laser employs an FDML laser, optical switch, and buffer stage. In the buffered FDML laser, part of the wavelength-swept light of the FDML laser is extracted by an optical switch and incident on the buffer stage, which is an optical system that branches into two optical paths with a delay fiber inserted in only one. Therefore, the wavelength-swept light can be multiplexed by combining lights emitted from the buffer stage. Using multiplexed wavelength-swept light, the developed buffered FDML laser is driven at a sweep rate of 50.7 kHz, producing a measurement rate of 202.8 kHz. Interrogation systems using buffered FDML lasers have the following advantages: simple optical manipulation using an optical switch and a buffer stage and high-speed performance surpassing the measurement rates of FDML lasers. In contrast, when using high-speed wavelength-swept lasers, the measurement accuracy is lowered owing to the influence of the delay. Therefore, a delay correction method from previous research [28], [30] was applied to the measurement using the buffered FDML laser. Reflection signals of FBGs were measured in real time by introducing a signal processing system mounted with an FPGA. We demonstrate that the interrogation system with the buffered FDML laser can measure reflection wavelengths of multiple FBGs with a time resolution of 4.9 μs without being affected by a delay.

II. Experimental Setup

A. FBG Interrogation System With Buffered FDML Laser

Fig. 1 shows the FBG interrogation system with a buffered FDML laser. The latter uses an FDML laser, optical amplifier (O-AMP), optical fiber switch (FSW), and buffer stage. The FDML laser is an optical fiber ring resonator type laser that employs a semiconductor optical amplifier, a fiber Fabry–Perot tunable filter (FFP-TF), and an optical fiber of 4 km (SMF-28, Corning) [28]. The semiconductor optical amplifier (SOA1117, Thorlabs) acts as a gain medium for the laser. The FFP-TF (Micron Optics) has a bandwidth of 85 pm, a finesse of 2195, and a free spectral range of 190 nm. The FFP-TF can extract specific wavelengths and control the wavelength sweep of the laser. The temperatures of these optical components were maintained at a constant value of 25 °C via temperature control using a thermal chamber (SLC-25A, Mitsubishi Electric Engineering) [28].

The FFP-TF was controlled using an oscillator (OSC, 33612A, Agilent). The OSC sets the control signal V_S to a sinusoidal waveform with a sweep rate f_m of 50.7 kHz. The FDML laser had a center wavelength of 1550 nm and a sweep bandwidth of ∼60 nm.

Laser sweeping is performed from the short wavelength to the long wavelength direction (forward scan) and from the long wavelength to the short wavelength direction (backward scan). The light emitted from the FDML laser is amplified by an O-AMP (SOA1013, Thorlabs) and enters the FSW. The FSW (NSSW, Agiltron) has an on/off ratio of 39 dB and a repeat rate of DC to 500 kHz and is controlled by the pulse control signal V_P from OSC via a switch driver (Agiltron). The FSW adjusts the pulse width t_{PW} of ∼4.5 μs and extracts light in the central wavelength regions of each section of the forward and backward scans of the FDML laser. The extracted light is incident on the buffer stage.

The buffer stage was inserted a 1 km fiber into one of the optical paths, and the buffer delay time t_H was controlled to ∼4.9 μs $(= 1/4f_m)$. Therefore, when the sweep lights of the FDML laser extracted by the FSW are incident on the buffer stage, lights combined by the coupler (CP_2) are multiplexed owing to the difference in the propagation time of each optical path. The temperature of the buffer stage was controlled in a laboratory environment at around 23 °C. In this experiment, the FDML laser was driven at a sweep rate f_m of 50.7 kHz. By using a bidirectional scan of forward and backward scans of the FDML laser, the interrogation system could achieve a measurement rate of 101.4 kHz $(= 2f_m)$. In addition, the buffered FDML laser with the buffer stage doubles the forward and backward scans by multiplexing, allowing the interrogation system to achieve a measurement rate of 202.8 kHz $(= 4f_m)$.

The emitted light from the buffered FDML laser entered each FBG via a circulator (CR). $\mathrm{FBG}_K (K = 1 - 3)$ has Bragg wavelengths of 1540, 1550, and 1560 nm, reflectance of ∼80%, and full width at half maximum of ∼0.2 nm. Reflection lights from the FBGs are received by detector (D). Here, the reference position P_S of the interrogation system corresponds to the fiber length in which the sweep characteristics of the buffered FDML laser are measured in Section 3.A. Therefore, as shown in Fig. 1, delays occur depending on the fiber lengths from the P_S to each FBG sensor. The effect of delays was examined by adjusting the length of the offset fiber (OF).

Reflection signals from FBGs were input to the ADC (NI5170R, National Instruments) equipped with an FPGA. The ADC had a sampling frequency of 250 MHz and a resolution of 14 bits. The ADC controls the recording timing by inputting the trigger signal V_T and reference clock V_R of the OSC. The acquired data were transferred to the FPGA. The FPGA implements peak detection with the centroid method and processes the detection of the peak signals of FBGs in real time. Then, the delay correction method, introduced in the next section, is applied to the peak signals of FBGs. Through a series of processes, the interrogation system with the buffered FDML laser can measure multiple FBGs with a time resolution of 4.9 μs $(= 1/4f_m)$ without being affected by delays.

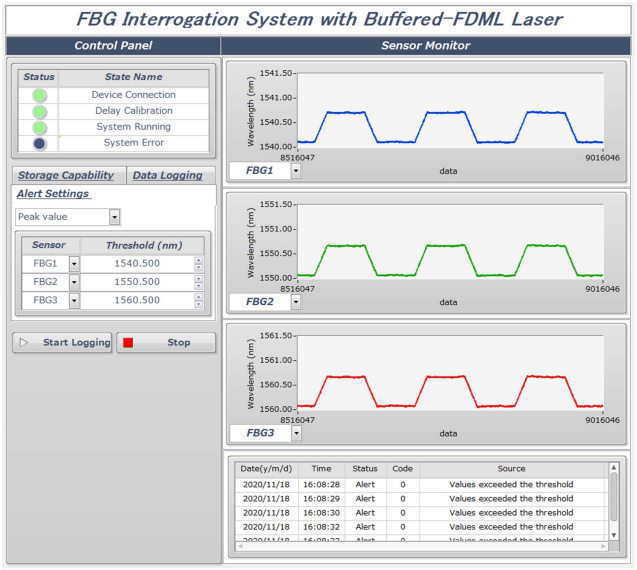

Fig. 2. Display screen for FBG interrogation system.

Fig. 2 shows the display screen of the interrogation system, which was developed using a programming language (LabVIEW, National Instruments). The interrogation system first corrects the delay, and when this is complete, measures the reflection wavelengths of multiple FBGs in real time. High-speed measurement data are saved in the technical data management streaming (TDMS) format (National Instruments) in binary format with high readability for high-speed and low-capacity storage. This enables real-time monitoring of the reflection wavelengths from multiple FBGs while storing them for a long time.

B. Measurement Method for FBGs With Buffered FDML Laser

This section compares measurement methods for FBGs using a general wavelength-swept laser including an FDML laser and using a buffered FDML laser, and describes how to apply delay correction. Fig. 3(I) shows the method for measuring the FBG using a wavelength-swept laser. First, it is assumed that the FBG is installed at the reference position P_S, as shown in Fig. 1, there is no delay, and the Bragg wavelength is λ_S. The wavelength-swept laser was driven by a sinusoidal signal at a sweep rate f_m and sweep interval T_m $(= 1/f_m)$. As shown in Fig. 3(I-a), the wavelength-swept laser sweeps in both the forward and backward scans. When the sweep wavelengths of the forward and backward scans match the Bragg wavelength of the FBG, the reflection signals of the FBG are detected at reflection times $t_S^{(F1)}$ and $t_S^{(B1)}$ [Fig. 3(I-b)]. The reflection wavelengths of the FBG can be measured by substituting the reflection times $t_S^{(F1)}$ and $t_S^{(B1)}$ into the wavelength sweep characteristics $f_{F1}(t)$ and $f_{B1}(t)$ of the forward and backward scans in the wavelength-swept laser. $f_{F1}(t)$ is the wavelength sweep characteristic with respect to time in the forward-scan region. $f_{B1}(t)$ is the wavelength sweep characteristic with respect to time in the backward-scan region. When using a bidirectional

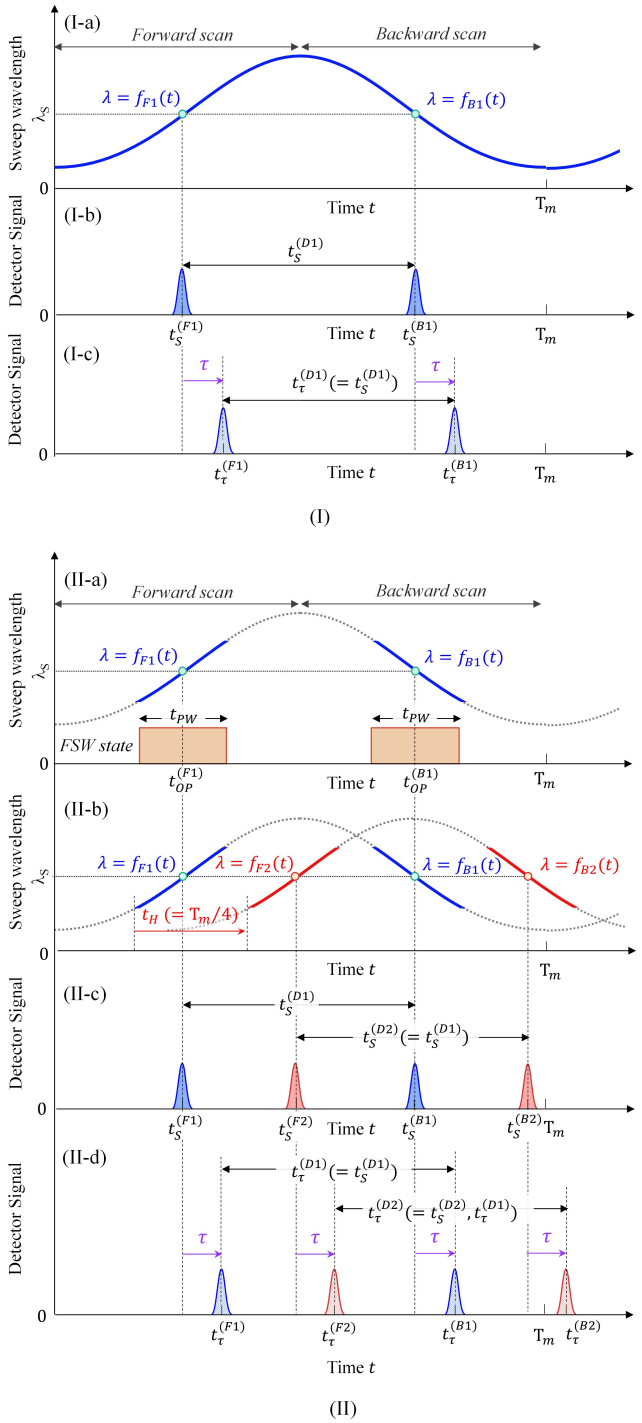

Fig. 3. FBG measurement with (I) general wavelength-swept laser and (II) buffered FDML laser. (I-a) Wavelength sweep of wavelength swept-laser. (I-b), (I-c) Reflection signals from FBG without and with delay. (II-a) Modulation of FDML laser with FSW. (II-b) Wavelength sweeping of buffered FDML laser. (II-c), (II-d) Reflection signals from FBG without and with delay.

wavelength sweep, the reflection wavelength was measured at every half of the sweep interval T_m.

However, when the FBG sensor is installed at a farther point than the reference position P_S, the reflection signals of the FBG are observed to shift to reflection times $t_\tau^{(F1)}$ and $t_\tau^{(B1)}$ under the influence of the delay τ, as shown in Fig. 3(I-c). Therefore, the converted reflection wavelengths also shift from the original FBG wavelength to the long wavelength side in the forward scan and to the short wavelength side in the backward scan. This problem can be solved by introducing a delay correction method with a bidirectional sweep of the wavelength-swept laser. The correction method measures the time difference $t_\tau^{(D1)}$ of the reflection times $t_\tau^{(F1)}$ and $t_\tau^{(B1)}$ obtained by the forward and backward scans. The time difference $t_\tau^{(D1)}$ can be used to calculate the delay τ because the delay terms of the reflection signals in the forward and backward scans cancel out, as shown in the following equation (see [28] and [30]).

$$t_\tau^{(D1)} = t_\tau^{(B1)} - t_\tau^{(F1)} = \left(t_S^{(B1)} + \tau\right) - \left(t_S^{(F1)} + \tau\right) \quad (1)$$

Therefore, the reflection times $t_S^{(F1)}$ and $t_S^{(B1)}$ can be determined by subtracting the delay τ from the reflection times $t_\tau^{(F1)}$ and $t_\tau^{(B1)}$ in the forward and backward scans.

To realize even faster measurement, Fig. 3(II) shows the measurement method using a buffered FDML laser. The buffered FDML laser modulates the optical fiber switch (FSW) with a pulse width $t_{PW} (< T_m/4)$ at pulse times $t_{OP}^{(F1)}$ and $t_{OP}^{(B1)}$ to extract light in the central wavelength regions of the forward and backward scans [Fig. 3(II-a)]. The extracted light is incident on the buffer stage. The buffer stage inserts a delay fiber into one of the optical paths and controls the buffer delay time $t_H (= T_m/4)$.

When the light extracted by the FSW is incident on the buffer stage, the wavelength-swept lights are multiplexed, as shown in Fig. 3(II-b). Therefore, the reflection signals of the FBG are detected at the reflection times $t_S^{(F1)}, t_S^{(F2)}, t_S^{(B1)}$, and $t_S^{(B2)}$ when the sweep wavelengths of the buffered FDML laser coincide with the Bragg wavelength [Fig. 3(II-c)]. The reflection wavelengths of the FBG can be calculated using the wavelength sweep characteristics $f_{F1}(t), f_{F2}(t), f_{B1}(t)$, and $f_{B2}(t)$. Here, $f_{F2}(t)$ is the wavelength sweep characteristic in the region where $f_{F1}(t)$ is shifted by the buffer delay time t_H. $f_{B2}(t)$ is the wavelength sweep characteristic in the region where $f_{B1}(t)$ is shifted by the buffer delay time t_H. With the buffered FDML laser, the reflection wavelengths can be measured at every quarter of the sweep interval T_m, which is twice as fast as a general wavelength-swept laser.

When affected by a delay in the buffered FDML laser, the reflection signals of the FBG by each wavelength sweep are shifted to reflection times $t_\tau^{(F1)}, t_\tau^{(F2)}, t_\tau^{(B1)}$, and $t_\tau^{(B2)}$ [Fig. 3(II-d)]. Time differences are expressed by two sets of equations (1) and (2), which can be used to calculate the delay τ.

$$t_\tau^{(D2)} = t_\tau^{(B2)} - t_\tau^{(F2)} = \left(t_S^{(B2)} + \tau\right) - \left(t_S^{(F2)} + \tau\right) \quad (2)$$

Therefore, even with the buffered FDML laser, the reflection times $t_S^{(F1)}, t_S^{(F2)}, t_S^{(B1)}$, and $t_S^{(B2)}$ can be determined by subtracting the delay τ from the reflection times $t_\tau^{(F1)}, t_\tau^{(F2)}, t_\tau^{(B1)}$, and $t_\tau^{(B2)}$ in the forward and backward scans. Our interrogation system uses a buffered FDML laser to correct the delay and measure the reflection wavelengths of the FBGs.

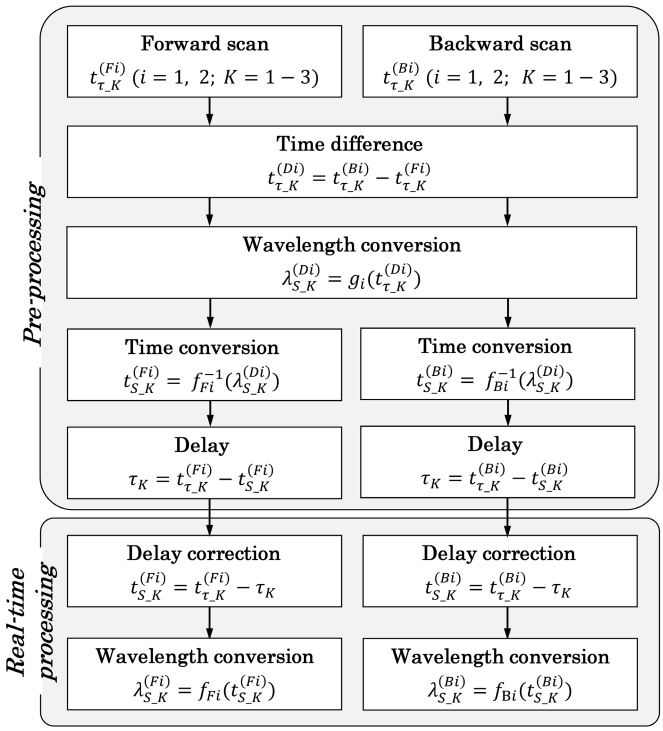

Fig. 4. Signal processing flow for measuring FBGs with delay correction.

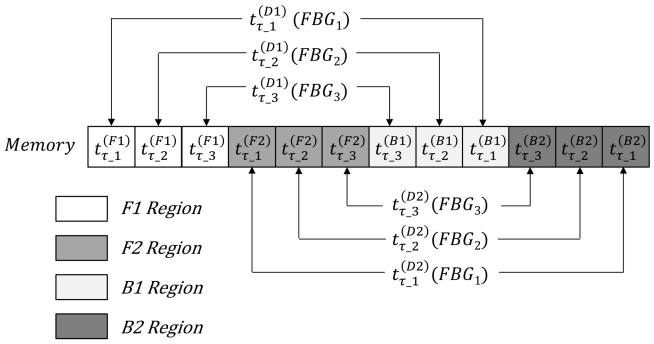

Fig. 5. Data of reflection times in PC memory.

C. Signal Processing With Delay Correction for Buffered FDML Laser

Fig. 4 shows the signal processing steps used for delay correction in our interrogation system. First, the wavelength swept lights of the buffered FDML laser are incident on each FBG$_K$ $(K = 1-3)$. Reflection signals of FBGs are acquired by the ADC, and reflection times $t_{\tau\_K}^{(Fi)}$ and $t_{\tau\_K}^{(Bi)}$ $(i = 1,2; K = 1-3)$ are detected by the FPGA. The reflection times of the FBGs are stored in the memory of the PC, as shown in Fig. 5. To perform delay correction, it is necessary to calculate the time differences using (1) and (2). In this experiment, the reflection times of each FBG were stored in order for each wavelength sweep region, as shown in Fig. 5. Then, the interrogation system calculates the time differences $t_{\tau\_K}^{(Di)}(i = 1,2; K = 1-3)$ from the reflection times $t_{\tau\_K}^{(Fi)}$ and $t_{\tau\_K}^{(Bi)}$ of the forward and backward scans.

The reflection wavelengths $\lambda_{S\_K}^{(Di)}(i = 1,2; K = 1-3)$ unaffected by delays can be calculated by substituting the time differences $t_{\tau\_K}^{(Di)}(i = 1,2; K = 1-3)$ into the wavelength sweep characteristics $g_i(t)$ $(i = 1,2)$ of the time differences (see [28] and [30]). Here, $g_1(t)$ is the wavelength sweep characteristic of the time difference by forward scan F1 and backward scan B1. $g_2(t)$ is the wavelength sweep characteristic of the time difference by forward scan F2 and backward scan B2. The calculated reflection wavelengths are substituted into the inverse functions $f_{Fi}^{-1}(\lambda)$ and $f_{Bi}^{-1}(\lambda)(i = 1,2)$ of the wavelength sweep characteristics $f_{Fi}(t)$ and $f_{Bi}(t)$, and the reflection times $t_{S\_K}^{(Fi)}$,$t_{S\_K}^{(Bi)}(i = 1,2; K = 1-3)$ of the FBGs are obtained. Therefore, delays $\tau_K(K = 1-3)$ can be calculated.

In real-time measurements, the reflection times $t_{\tau\_K}^{(Fi)}$ and $t_{\tau\_K}^{(Bi)}$ of FBGs affected by delays are measured, and delays τ_K calculated earlier are removed. Finally, the reflection times $t_{S\_K}^{(Fi)}$ and $t_{S\_K}^{(Bi)}$ are substituted into the wavelength sweep characteristics $f_{Fi}(t)$ and $f_{Bi}(t)$ $(i = 1,2)$ to calculate the reflection wavelengths $\lambda_{S\_K}^{(Fi)}$ and $\lambda_{S\_K}^{(Bi)}(i = 1,2; K = 1-3)$. By executing this series of processes, as the wavelength can be calculated by both the forward and backward scans of the buffered FDML laser, a measurement time resolution of 4.9 μs can be achieved.

III. Experimental Results

A. Characteristics of Buffered FDML Laser

To construct the buffered FDML laser, first, the output characteristics of the FDML laser were measured with the detector and optical spectrum analyzer.

Fig. 6(I-a) shows the time waveform of the FDML laser with amplification by the O-AMP. It can be seen that the FDML laser performs a forward scan (F1) and backward scan (B1) every half cycle of the sweep interval T_m, as shown in Fig. 3(I-a). Fig. 6(I-b) shows the output spectrum of the laser measured with the optical spectrum analyzer by averaging 10 times. The average number of times of the optical spectrum analyzer is set to 10 to secure a sufficient measurement time and to observe the average spectral behavior of the FDML laser. The FDML laser sweeps the wavelength in a sinusoidal manner at a sweep rate of 50.7 kHz. As the measurement speed of the optical spectrum analyzer is lower than the sweep speed of the laser, sharp peaks are observed at both ends of the output spectrum, similar to the probability density of a sinusoidal wave. The FDML laser had a center wavelength of 1550 nm and sweep bandwidth of ~60 nm. It is considered that the intensity noise of the time waveform can be reduced by performing dispersion compensation using a dispersion compensating fiber [42]. The average output power was ~4.2 mW measured by a power meter. It was confirmed that the FDML laser operated successfully at high speed with a sweep rate of 50.7 kHz.

Therefore, a buffered FDML laser was constructed by extracting part of the emitted light of the FDML laser with an optical switch (FSW) and a buffer stage. Fig. 6(II-a) and (II-b) show the time waveform and output spectrum, respectively. The FSW was modulated with a pulse width $t_{PW} \sim 4.5$ μs at pulse times $t_{OP}^{(F1)} \sim 4.9$ μs, $t_{OP}^{(B1)} \sim 14.7$ μs, extracting lights in the central wavelength regions of the forward scan (F1)

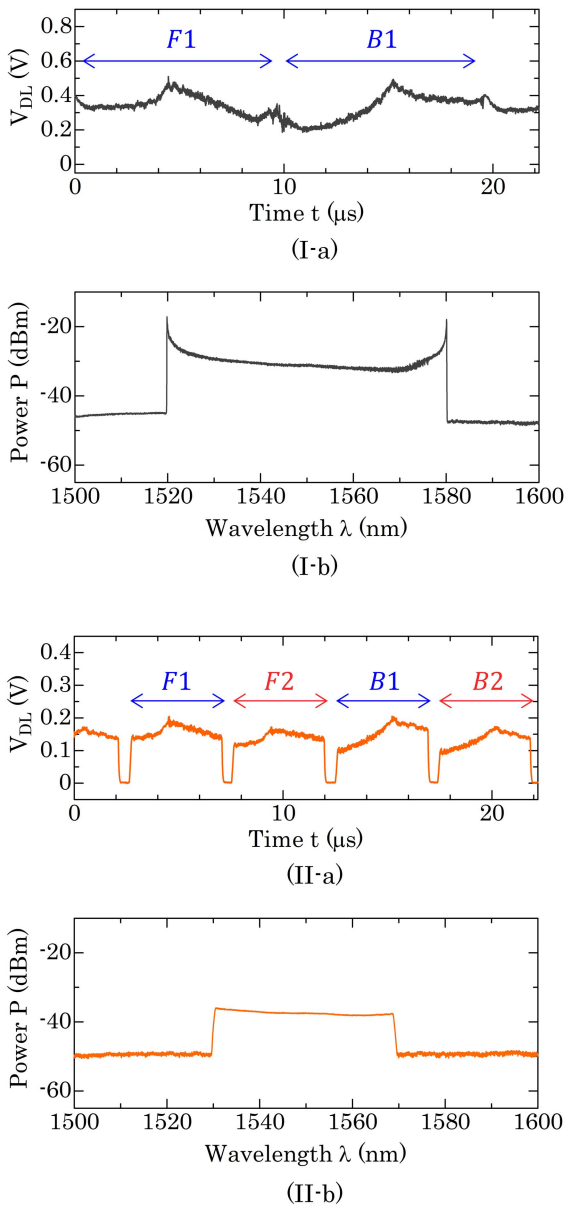

Fig. 6. Comparison of output lights for (I) FDML laser and (II) buffered FDML laser. (I-a) Time waveform of FDML laser. (I-b) Output spectrum of FDML laser. (II-a) Time waveform of buffered FDML laser. (II-b) Output spectrum of buffered FDML laser.

and backward scan (B1) of the FDML laser. Extracted lights entered the buffer stage with a buffer delay time t_H. Thus, the optical outputs of the forward scan (F2) and backward scan (B2) can be obtained in the regions where the forward scan (F1) and backward scan (B1) were delayed by the buffer delay time t_H, as shown in Fig. 6(II-a). The buffered FDML laser had a sweep bandwidth of ∼39 nm. As shown in Fig. 3 (II-a), when the FDML laser sweeps in a sinusoidal wave with a sweep bandwidth of 60 nm, the light extracted by FSW ($t_{PW} \sim 4.5\ \mu$s) is a part of the central wavelength region. Therefore, the buffered FDML laser reduces the sweep bandwidth from 60 nm to 39 nm. The buffered FDML laser can multiplex the wavelength-swept light in the buffer stage, allowing the wavelength to be swept at every quarter of the sweep interval T_m.

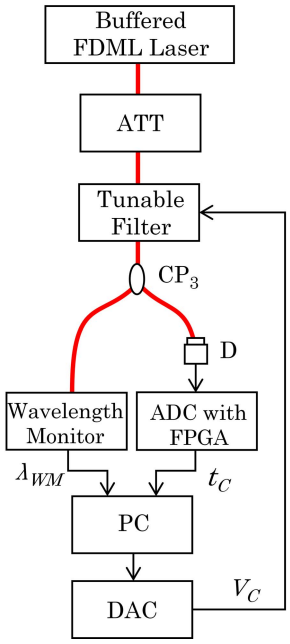

Fig. 7. Experimental system for measuring wavelength sweep characteristics of buffered FDML laser.

To measure the reflection wavelengths of the FBGs using the buffered FDML laser, the wavelength sweep characteristics $f_{Fi}(t)$ and $f_{Bi}(t)$ $(i = 1, 2)$ were measured [28]. Fig. 7 shows an experimental system for measuring the wavelength-sweep characteristics of the buffered FDML laser. The system injects the emitted light from the buffered FDML laser into a tunable filter via an attenuator (ATT). The tunable filter (FFM-C, Axsun Technologies) extracts only the light in a specific wavelength region from the buffered FDML laser. The tunable filter was tuned by the control signal V_C of a digital-to-analog converter (DAC).

The extracted light is incident on the detector and the wavelength monitor, and the relationship between the detected time t_C and wavelength λ_{WM} was measured for the wavelength-sweep characteristics. The wavelength monitor (FB200, ANDO) is a spectroscopic instrument with a measurement range of 1527–1567 nm, time resolution of 10 ms, wavelength resolution of 1 pm, and measurement accuracy of ±50 pm. The wavelength sweep characteristics of the buffered FDML laser were measured at 690 sampling points by controlling the tunable filter.

Fig. 8(a) shows the results of measuring the wavelength sweep characteristics of the buffered FDML laser. The wavelength sweep characteristics $f_{F1}(t)$ and $f_{B1}(t)$ of the forward scan (F1) and backward scan (B1) can be measured. Furthermore, by using the buffer stage, the wavelength sweep characteristics $f_{F2}(t)$ and $f_{B2}(t)$ of the multiplexed forward scan (F2) and backward scan (B2) can be measured. It can be seen that the buffered FDML laser performs multiple wavelength sweeps, as shown in Fig. 3(II-b).

To correct the delay, the wavelength sweep characteristics $g_1(t)$ and $g_2(t)$ of the time differences were calculated from the wavelength sweep characteristics $f_{F1}(t)$ and $f_{B1}(t)$ and the wavelength sweep characteristics $f_{F2}(t)$ and $f_{B2}(t)$,

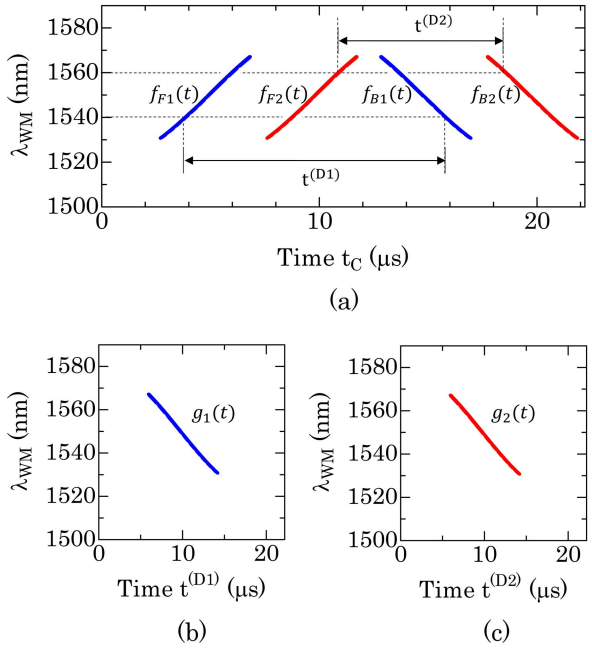

Fig. 8. Wavelength sweep characteristics of buffered FDML laser. (a) Characteristics of multiple wavelength sweeps. (b) and (c) Characteristics of $g_1(t)$ and $g_2(t)$ of time differences.

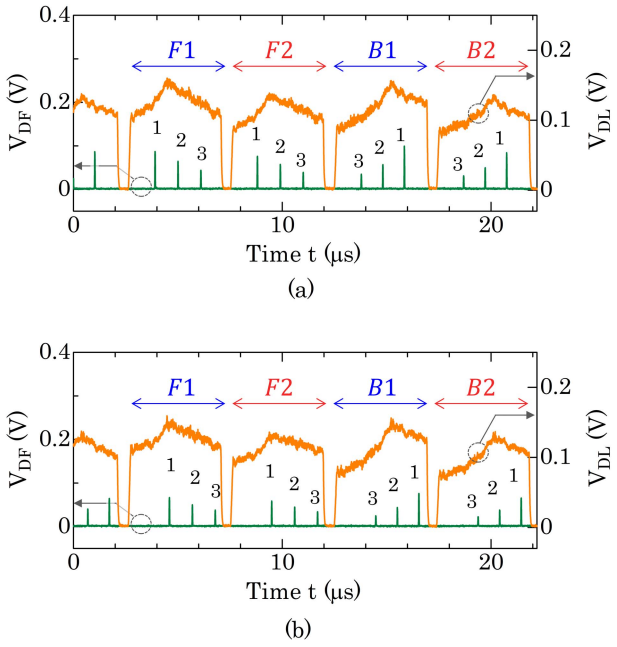

Fig. 9. Reflection signals of FBGs with buffered FDML laser. (a) $\Delta L_{OF} = 0$ m; (b) $\Delta L_{OF} = 70$ m.

respectively [Fig. 8(b) and (c)]. The time difference $t^{(D1)}$ was calculated by obtaining the time difference when the wavelengths of the wavelength sweep characteristics $f_{F1}(t)$ and $f_{B1}(t)$ were the same. Because the relationship between the time difference $t^{(D1)}$ and the wavelength could be obtained, the wavelength sweep characteristic $g_1(t)$ of the time difference could be calculated as shown in Fig. 8 (b). The wavelength sweep characteristic $g_2(t)$ of the time difference $t^{(D2)}$ was calculated in the same way. Wavelength sweep characteristics $g_1(t)$ and $g_2(t)$ of the time differences were changed wavelengths depending on the time differences $t^{(D1)}$ and $t^{(D2)}$. The standard deviation of the difference of the wavelength sweep characteristics $g_1(t)$ and $g_2(t)$ at the same wavelength were less than 0.71 ns. Almost identical characteristics were observed. In the next section, the wavelength sweep characteristics of the buffered FDML laser are used to measure FBGs with the effects of delays removed.

B. FBGs Measurements With Delay Correction for Buffered FDML Laser

The emission light of the buffered FDML laser was incident on the FBGs, and the reflection signals of the FBGs were measured. The offset fiber (OF) shown in Fig. 1 was set to a fiber length of $\Delta L_{OF} = 0$ m. Fig. 9(a) shows the results of the reflection signals V_{DF} of the FBGs and output signal V_{DL} of the buffered FDML laser. By using the buffered FDML laser, the reflection signals of each FBG can be detected for each wavelength sweep, resulting in a measurement interval of 4.9 μs. Reflection signals of FBG_1 in forward scans F1 and F2 were $t_{\tau\_1}^{(F1)} = 3.91$ μs and $t_{\tau\_1}^{(F2)} = 8.81$ μs, respectively, and were delayed by the buffer delay time t_H. Therefore, while the design target value of the buffer delay time t_H was 4.93 μs $(= 1/4f_m)$, this measurement system could control it to 4.90 μs. For a fiber length of $\Delta L_{OF} = 0$ m, reflection signals of each FBG in the forward scan (F1) were $t_{\tau\_1}^{(F1)} = 3.91$ μs, $t_{\tau\_2}^{(F1)} = 5.01$ μs, and $t_{\tau\_3}^{(F1)} = 6.10$ μs.

In order to examine the effect of the delay, the OF was set to $\Delta L_{OF} = 70$ m, and the reflection signals of FBGs were measured. Fig. 9(b) shows the results for $\Delta L_{OF} = 70$ m, and the reflection signals of the FBGs were detected with a delay later than in the case of Fig. 9(a). Reflection signals of FBG_1 in forward scans F1 and F2 were $t_{\tau\_1}^{(F1)} = 4.60$ μs and $t_{\tau\_1}^{(F2)} = 9.50$ μs, respectively. Because the delay per unit length of an optical fiber is approximately 9.8 ns, a fiber length of 70 m is equivalent to 0.69 μs. For a fiber length of $\Delta L_{OF} = 70$ m, reflection signals of each FBG in the forward scan (F1) were $t_{\tau\_1}^{(F1)} = 4.60$ μs, $t_{\tau\_2}^{(F1)} = 5.70$ μs, and $t_{\tau\_3}^{(F1)} = 6.79$ μs. Although the reflection signal of each FBG was shifted owing to the increase in the delay due to the longer fiber, the relative intervals among the three peaks of FBGs were the same. When a delay occurs, the reflection signals of FBGs are shifted and observed, and the converted reflection wavelengths also shift from the original wavelengths of the FBGs. By correcting the delay based on the signal processing in Fig. 4, the interrogation system can calculate the original wavelength from the wavelength sweep characteristic of Fig. 8.

Therefore, the reflection wavelengths of the FBGs in the applied strain were measured using the delay correction method, as shown in Fig. 4. To apply strain, both ends of the optical-fiber-installed FBG_3 were attached to a fixed stage and a movable stage with a spacing of $L_I = 1$ m. The movable stage had a moving speed of 5000 μm/s. A tensile strain $\Delta\varepsilon_3 (= \Delta X_3 / L_I)$ was applied by moving the stage by $\Delta X_3 \mu$m in the axial direction of the optical fiber.

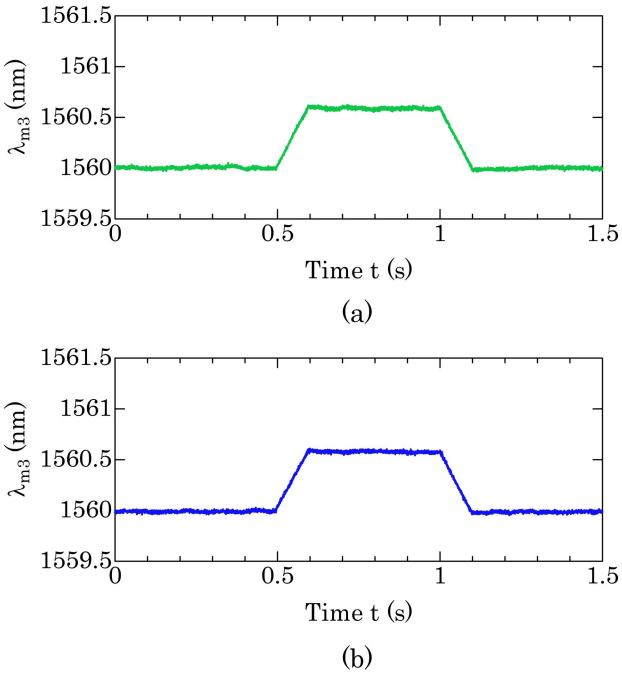

Fig. 10. Dynamic strain measurement with delay correction. (a) $\Delta L_{OF} = 0$ m; (b) $\Delta L_{OF} = 70$ m.

Fig. 10(a) shows the result of measuring the reflection wavelength by applying a dynamic strain $\Delta\varepsilon_3 = 500\ \mu\varepsilon$ to FBG_3. The installation position of FBG_3 was set to 9.71 m with $\Delta L_{OF} = 0$ m, and the reflection wavelengths before and after strain application were 1560.00 nm and 1560.59 nm, respectively. Fig. 10(b) shows the result when $\Delta L_{OF} = 70$ m. Values of reflection wavelengths before and after strain application were 1559.99 nm and 1560.58 nm, respectively. The reflection wavelength of FBG_3 owing to strain can be measured without being affected by the delay.

Fig. 11 shows the results with and without delay correction and provides an enlarged view of Fig. 10 near t = 0 s. The reflection wavelength without delay correction was calculated by ignoring the delay term of delay correction in Fig. 4. For a fiber length of $\Delta L_{OF} = 0$ m (Fig. 11(a)), the installation position of FBG_3 was set to 9.71 m. The reflection wavelengths without delay correction shifted from the original wavelength to the long wavelength side during the forward scans and to the short wavelength side during the backward scans. The reflection wavelengths in each scan were $\lambda_{S\_3}^{(F1)} = 1560.79$ nm, $\lambda_{S\_3}^{(F2)} = 1560.79$ nm, $\lambda_{S\_3}^{(B1)} = 1559.20$ nm, and $\lambda_{S\_3}^{(B2)} = 1559.19$ nm. When the delay was corrected, the reflection wavelengths in each scan had the same value of 1560. 00 nm. For a fiber length of $\Delta L_{OF} = 70$ m (Fig. 11(b)), the reflection wavelength of each scan without delay correction shifted greater than the case of $\Delta L_{OF} = 0$ m owing to the increase in the delay due to the longer fiber. The reflection wavelengths in each scan with delay correction were almost 1559.99 nm. Even if the effect of delay changes, the interrogation system can remove the delay and measure the reflection wavelength.

Therefore, the reflection wavelength of FBG_3 was measured over a wide strain range of 0–2000 $\mu\varepsilon$. In addition, the

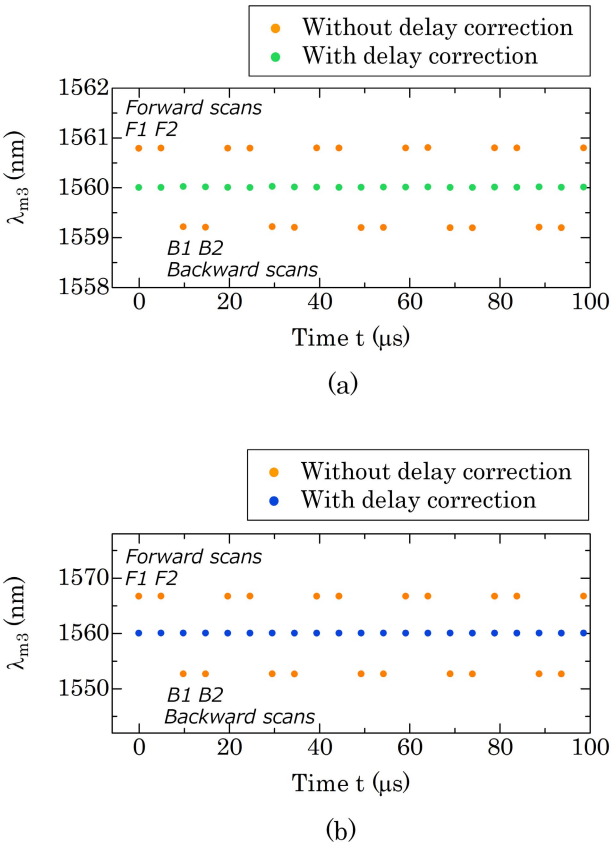

Fig. 11. Enlarged view of Fig. 10 with and without delay correction. (a) $\Delta L_{OF} = 0$ m; (b) $\Delta L_{OF} = 70$ m.

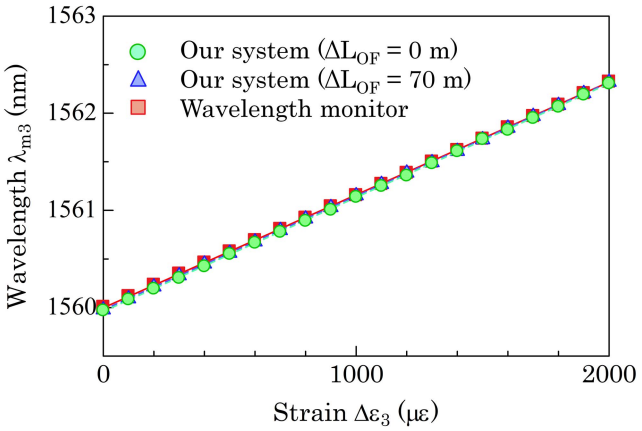

Fig. 12. Reflection wavelengths in wide range of strain with delay correction.

measurement was performed in comparison with a wavelength monitor (FB200, ANDO). Fig. 12 shows the results of measuring the reflection wavelengths by applying static strains to FBG_3 with $\Delta L_{OF} = 0$ and 70 m. For $\Delta L_{OF} = 0$ m, it is possible to measure how the reflection wavelength changes in proportion to the strain. Even when $\Delta L_{OF} = 70$ m, the same wavelength change as $\Delta L_{OF} = 0$ m can be measured without being affected by the delay. The standard deviation of the difference of reflection wavelengths at $\Delta L_{OF} = 0$ and 70 m was 8.4 pm.

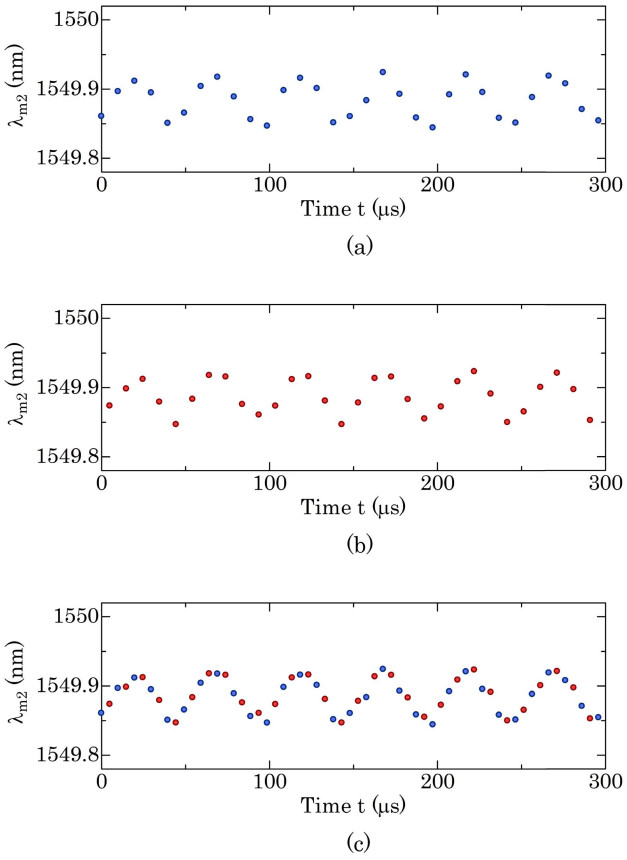

Fig. 13. Vibration measurement with buffered FDML laser. (a) Measurement by using forward scan (F1) and backward scan (B1). (b) Measurement by using forward scan (F2) and backward scan (B2). (c) Measurement by combining (a) and (b).

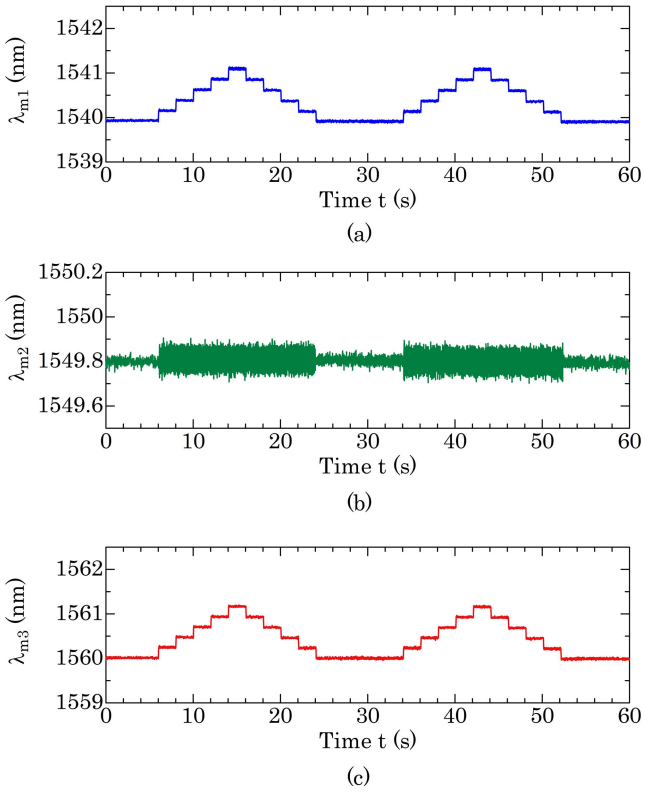

Fig. 14. Measurements at high speed and in real time. (a) FBG_1, (b) FBG_2, (c) FBG_3.

Furthermore, the results of this interrogation system were in good agreement with the measured values of the wavelength monitor. The slope of the reflection wavelength with respect to strain in our interrogation system was 1.17×10^{-3} nm/$\mu\varepsilon$ ($R^2 = 0.99992$) at each ΔL_{OF}. The maximum difference between the approximate expression and the measured value was 15 pm. The slope in the wavelength monitor was 1.16×10^{-3} nm/$\mu\varepsilon$. In this experiment, the maximum difference between the measured values of our interrogation system and the wavelength monitor was 44 pm. From the above results, our interrogation system can measure the reflection wavelength with the delay removed using a buffered FDML laser.

C. Real-Time Measurement With Buffered FDML Laser

The high-speed vibration was measured using an interrogation system with a buffered FDML laser. FBG_2 was attached to a steel case of a metal-sealed multilayer piezoelectric actuator. The vibration was produced by a piezo actuator driven at a vibration frequency of 20 kHz. The installation position of FBG_2 was set to 6.39 m with $\Delta L_{OF} = 0$ m.

Fig. 13(a) shows the results measured using the forward scan (F1) and backward scan (B1). This is the same condition as a general FBG measurement using forward and backward scans of the FDML laser, as shown in Fig. 3(I). For each scan, the vibration waveform in the reflection wavelength can be measured at a measurement interval of 9.9 μs. However, the waveform in the vibration was unclear owing to insufficient sampling in the measurement by each scan. Therefore, it is necessary to increase the measurement rate to detect high-speed vibrations of several tens of kHz.

Fig. 13(b) shows the results of the forward scan (F2) and backward scan (B2) produced by introducing the buffered FDML. Compared to the measurement using forward scan (F1) and backward scan (B1), the measurement interval was equal; however, the sampling timing was delayed by the buffer delay time t_H.

Therefore, by combining the above two types of sweeps, measurements using the buffered FDML laser were carried out, as shown in Fig. 13(c). The buffered FDML laser improved the measurement interval to 4.9 μs. The change in the reflection wavelength owing to vibration can be measured for each sweep. By improving the measurement rate to more than 10 times the vibration frequency, it can be clearly seen that the reflection wavelength vibrates periodically with a sinusoidal wave. The fluctuation of the reflection wavelength in the vibration was ~70 pm. From the above results, the interrogation system using the buffered FDML laser can improve the measurement rate and capture high-speed vibrations.

Real-time measurements of the reflection wavelengths from FBGs were performed using the interrogation system. Movable stages were attached to FBG_1 and FBG_3, and strains of 200 $\mu\varepsilon$ were applied in steps every 2 s. FBG_2 was attached to a piezoelectric vibrator with a resonance frequency of 4.64 kHz, and vibration was applied.

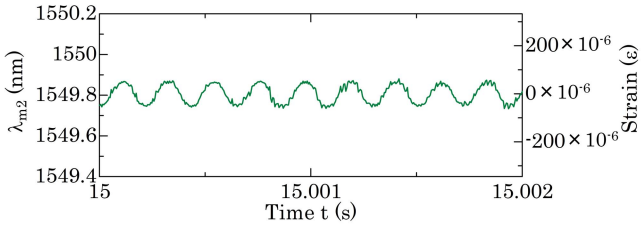

Fig. 15. Enlarged view of Fig. 14(b).

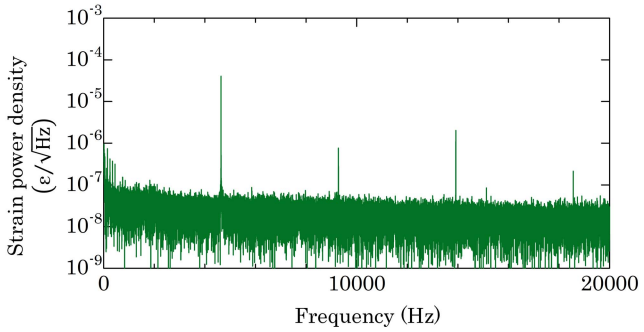

Fig. 16. Power spectral density of FBG_2.

Fig. 14 shows the results of real-time measurements of the reflection wavelengths for 60 s. More than 12 million data points per FBG were continuously acquired at high speed in real time. FBG_1 and FBG_3 showed changes in reflection wavelengths of ∼0.23 nm owing to step-like strains. The reflection wavelength of FBG_2 fluctuated greatly because of the application of vibration at t = 6 and 34 s. The standard deviations of the reflection wavelengths in the section where strain and vibration were not applied in each FBG were less than 12 pm. The interrogation system can simultaneously measure the reflection wavelengths of multiple FBGs owing to strain and vibration in real time. In addition, the effects of delays in each FBG were removed and measured. According to the results of FBG_1 for 1 min, the measurement wavelengths at the start and at the end of the measurement were 1539.92 nm and 1539.91 nm, respectively, indicating that the system could perform stable measurements.

Fig. 15 shows the result of expanding the time domain of FBG_2 in Fig. 14 (b) near t = 15 s. The value of the reflection wavelength fluctuated at a vibration frequency of 4.64 kHz. The peak-to-peak value in fluctuation was ∼0.12 nm. In Fig. 15, the peak-to-peak value converted to strain corresponds to ∼100 $\mu\varepsilon$. The root mean square (RMS) value of the strain calculated from the time waveform was ∼37 $\mu\varepsilon$.

Fig. 16 shows the result of the power spectral density [43] around 15 s in Fig. 15. The power spectral density analysis used 262144 data (∼1.29 s). The sharp peak with a vibration frequency of 4.64 kHz was almost the same as the RMS in the time domain. The strain sensitivity estimated by the noise floor was ∼50 n$\varepsilon/\sqrt{\text{Hz}}$. The 4.64 kHz harmonics were due to the non-linearity of the piezoelectric vibrator. The interrogation system can measure multiple FBGs with a time resolution of 4.9 μs over 60 s without being affected by delays.

IV. Conclusion

In this study, we developed a high-speed interrogation system with a buffered FDML laser for sensing multiple FBGs. The buffered FDML laser multiplexed the wavelength-swept light using an optical switch and a buffer stage. This operation made it possible to achieve twice the measurement rate of the FDML laser alone. The buffered FDML laser was driven at a sweep rate of 50.7 kHz with a bandwidth of ∼39 nm. The interrogation system achieved a measurement rate of 202.8 kHz with the buffered FDML laser. Bidirectional wavelength sweeps of the buffered FDML laser were used to construct the signal processing that eliminated the effects of delays. The interrogation system was equipped with ADC and FPGA with a sampling frequency of 250 MHz and performed real-time calculation of reflection wavelengths of FBGs. It was demonstrated that the interrogation system can measure the reflection wavelengths of multiple FBGs with a time resolution of 4.9 μs by eliminating the effects of delays over 60 s. To the best of our knowledge, as a multipoint and real-time interrogation system using a wavelength-swept laser, it has the highest measurement time resolution for calculating reflection wavelengths of multiple FBGs. This paper demonstrates that the interrogation system can stably measure over 12 million reflection wavelength data per FBG per minute in real time. In addition, the interrogation system has the ability to correct the effects of delay, which is a major challenge in high-speed FBG measurements.

Buffered FDML lasers can further increase measurement rates several times by increasing the number of branches in the buffer stage. Therefore, the measurement method using a buffered FDML laser can potentially enable the development of faster FBG interrogation systems by increasing the measurement rate of existing FDML lasers by several times using simple optical manipulations. We plan to develop a new buffered FDML laser with an adjusted number of optical paths in the buffer stage and design a high-speed digital signal processing for detecting FBGs.

References

[1] R. Huber, M. Wojtkowski, K. Taira, J. G. Fujimoto, and K. Hsu, "Amplified, frequency swept laser for frequency domain reflectometry and OCT imaging: Design and scaling principles," *Opt. Exp.*, vol. 13, no. 9, pp. 3513–3528, May 2005.

[2] R. Huber, M. Wojtkowski, and J. G. Fujimoto, "Fourier Domain Mode Locking (FDML): A new laser operating regime and applications for optical coherence tomography," *Opt. Exp.*, vol. 14, no. 8, pp. 3225–3237, Apr. 2006.

[3] C. M. Eigenwillig *et al.*, "Picosecond pulses from wavelength-swept continuous-wave Fourier domain mode-locked lasers," *Nature Commun.*, vol. 4, no. 1, pp. 1–7, May 2013.

[4] L. A. Kranendonk *et al.*, "High speed engine gas thermometry by Fourier-domain mode-locked laser absorption spectroscopy," *Opt. Exp.*, vol. 15, no. 23, pp. 15115–15128, Nov. 2007.

[5] E. J. Jung *et al.*, "Characterization of FBG sensor interrogation based on a FDML wavelength swept laser," *Opt. Exp.*, vol. 16, no. 21, pp. 16552–16560, Oct. 2008.

[6] D. Chen, C. Shu, and S. He, "Multiple fiber Bragg grating interrogation based on a spectrum-limited Fourier domain mode-locking fiber laser," *Opt. Lett.*, vol. 33, no. 13, pp. 1395–1397, Jul. 2008.

[7] B. C. Lee, E. J. Jung, C. S. Kim, and M. Y. Jeon, "Dynamic and static strain fiber Bragg grating sensor interrogation with a 1.3 μm Fourier domain mode-locked wavelength-swept laser," *Meas. Sci. Technol.*, vol. 21, no. 9, Jul. 2010, Art. no. 094008.

[8] Q. Liu *et al.*, "High-speed interrogation system of multi-encoding weak FBGs based on FDML wavelength swept laser," *Opt. Laser Technol.*, vol. 107, pp. 54–58, Nov. 2018.

[9] E. J. Friebele *et al.*, "Optical fiber sensors for spacecraft applications," *Smart Mater. Struct.*, vol. 8, no. 6, pp. 813–838, Dec. 1999.

[10] M. D. Todd, G. A. Johnson, and B. L. Althouse, "A novel Bragg grating sensor interrogation system utilizing a scanning filter, a Mach-Zehnder interferometer and a 3×3 coupler," *Meas. Sci. Technol.*, vol. 12, no. 7, pp. 771–777, Jan. 2001.
[11] K. Hotate and Z. He, "Synthesis of optical-coherence function and its applications in distributed and multiplexed optical sensing," *J. Lightw. Technol.*, vol. 24, no. 7, pp. 2541–2557, Jul. 2006.
[12] Y. Shinoda, T. Arai, D. Miyata, and T. Higo, "Real-time measurement of static strain using fiber Bragg gratings with optical frequency domain reflectometry," in *Proc. SICE Ann. Conf.*, Sep. 2011, pp. 1870–1873.
[13] A. Wada, S. Tanaka, and N. Takahashi, "Optical fiber vibration sensor using FBG Fabry–Perot interferometer with wavelength scanning and Fourier analysis," *IEEE Sensors J.*, vol. 12, no. 1, pp. 225–229, Jan. 2012.
[14] K. Yuksel, V. Moeyaert, P. Megret, and M. Wuilpart, "Complete analysis of multireflection and spectral-shadowing crosstalks in a quasi-distributed fiber sensor interrogated by OFDR," *IEEE Sensors J.*, vol. 12, no. 5, pp. 988–995, May 2012.
[15] Y. Mizuno, N. Hayashi, H. Fukada, K. Y. Song, and K. Nakamura, "Ultrahigh-speed distributed Brillouin reflectometry," *Light: Sci. Appl.*, vol. 5, no. 12, Jun. 2016, Art. no. e16184.
[16] M. Zhu and H. Murayama, "Fast demodulation of OFDR based long length FBG sensing system for noisy signals," *Opt. Exp.*, vol. 26, no. 16, pp. 19804–19814, Aug. 2018.
[17] X. Liang *et al.*, "Precision dynamic sensing with ultra-weak fiber Bragg grating arrays by wavelength to frequency transform," *J. Lightw. Technol.*, vol. 37, no. 14, pp. 3526–3531, Jul. 15, 2019.
[18] R. Cheng, L. Xia, Y. Ran, J. Rohollahnejad, J. Zhou, and Y. Wen, "Interrogation of ultrashort Bragg grating sensors using shifted optical Gaussian filters," *IEEE Photon. Technol. Lett.*, vol. 27, no. 17, pp. 1833–1836, Sep. 1, 2015.
[19] Á. González-Vila, D. Kinet, P. Mégret, and C. Caucheteur, "Narrowband interrogation of plasmonic optical fiber biosensors based on spectral combs," *Opt. Laser Technol.*, vol. 96, pp. 141–146, Nov. 2017.
[20] J. Guo, Y. Ding, X. Xiao, L. Kong, and C. Yang, "Multiplexed static FBG strain sensors by dual-comb spectroscopy with a free running fiber laser," *Opt. Exp.*, vol. 26, no. 13, pp. 16147–16154, Jun. 2018.
[21] J. M. Lopez-Higuera, *Handbook of Optical Fibre Sensing Technology*. Hoboken, NJ, USA: Wiley, 1997.
[22] A. Kersey *et al.*, "Fiber grating sensors," *J. Lightw. Technol.*, vol. 15, no. 8, pp. 1442–1463, Aug. 1997.
[23] A. Othonos and K. Kalli, *Fiber Bragg Gratings*. Norwood, MA, USA: Artech House, 1999.
[24] J. M. López-Higuera, L. Rodriguez-Cobo, A. Q. Incera, and A. Cobo, "Fiber optic sensors in structural health monitoring," *J. Lightw. Technol.*, vol. 29, no. 4, pp. 587–608, Feb. 15, 2011.
[25] S. H. Yun, D. J. Richardson, and B. Y. Kim, "Interrogation of fiber grating sensor arrays with a wavelength-swept fiber laser," *Opt. Lett.*, vol. 23, no. 11, pp. 843–845, 1998.
[26] T. Saitoh, K. Nakamura, Y. Takahashi, H. Iida, Y. Iki, and K. Miyagi, "Ultra-long-distance fiber Bragg grating sensor system," *IEEE Photon. Technol. Lett.*, vol. 19, no. 20, pp. 1616–1618, Oct. 15, 2007.
[27] R. Isago and K. Nakamura, "A high reading rate fiber Bragg grating sensor system using a high-speed swept light source based on fiber vibrations," *Meas. Sci. Technol.*, vol. 20, no. 3, Feb. 2009, Art. no. 034021.
[28] T. Yamaguchi and Y. Shinoda, "Real-time fiber Bragg grating measurement system using temperature-controlled Fourier domain mode locking laser," *Opt. Eng.*, vol. 56, no. 6, Jun. 2017, Art. no. 066112.
[29] T. Yamaguchi and Y. Shinoda, "Multichannel high-speed fiber Bragg grating interrogation system utilizing a field programmable gate array," *IEEE Sensors Lett.*, vol. 2, no. 1, pp. 1–4, Mar. 2018.
[30] T. Yamaguchi, K. Ishihara, and Y. Shinoda, "Field-programmable gate array-based multichannel measurement system for interrogating fiber Bragg grating sensors," *IEEE Sensors J.*, vol. 19, no. 15, pp. 6163–6172, Aug. 2019.
[31] Z. Li, M. Liu, Y. Wang, Q. Liu, and J. Gong, "Delay calibration method for wavelength-swept laser-based FBG demodulation system," *IEEE Photon. Technol. Lett.*, vol. 26, no. 20, pp. 2090–2092, Oct. 15, 2014.
[32] J. Mei, X. Xiao, and C. Yang, "Delay compensated FBG demodulation system based on Fourier domain mode-locked lasers," *IEEE Photon. Technol. Lett.*, vol. 27, no. 15, pp. 1585–1588, Aug. 1, 2015.
[33] X. Liang, Z. Li, Y. Wang, Y. Hou, and P. Shen, "Delay-disorder fiber Bragg grating recognition and calibration method for a Fourier domain mode-locked wavelength-swept laser-based interrogation system," *Appl. Opt.*, vol. 57, no. 28, pp. 8148–8153, Oct. 2018.
[34] T. Yamaguchi, W. Endo, and Y. Shinoda, "Interrogation system with automatic recognition and delay correction functions of fiber Bragg gratings by pulse modulation with wavelength-swept laser," *IEEE Sensors J.*, vol. 19, no. 22, pp. 10519–10528, Nov. 2019.
[35] N. Takeda, Y. Okabe, J. Kuwahara, S. Kojima, and T. Ogisu, "Development of smart composite structures with small-diameter fiber Bragg grating sensors for damage detection: Quantitative evaluation of delamination length in CFRP laminates using Lamb wave sensing," *Compos. Sci. Technol.*, vol. 65, nos. 15–16, pp. 2575–2587, Dec. 2005.
[36] H. Tsuda *et al.*, "Acoustic emission measurement using a strain-insensitive fiber Bragg grating sensor under varying load conditions," *Opt. Lett.*, vol. 34, no. 19, pp. 2942–2944, Oct. 2009.
[37] G. Wild and S. Hinckley, "Acousto-ultrasonic optical fiber sensors: Overview and state-of-the-art," *IEEE Sensors J.*, vol. 8, no. 7, pp. 1184–1193, Jul. 2008.
[38] K. S. Kim, Y. Mizuno, and K. Nakamura, "Fiber-optic ultrasonic hydrophone using short Fabry–Perot cavity with multilayer reflectors deposited on small stub," *Ultrasonics*, vol. 54, no. 4, pp. 1047–1051, Apr. 2014.
[39] Q. Rong *et al.*, "Ultrasonic imaging of seismic physical models using fiber Bragg grating Fabry–Perot probe," *IEEE J. Sel. Topics Quantum Electron.*, vol. 23, no. 2, pp. 223–228, Apr. 2017.
[40] R. Huber, D. C. Adler, and J. G. Fujimoto, "Buffered Fourier domain mode locking: Unidirectional swept laser sources for optical coherence tomography imaging at 370,000 lines/s," *Opt. Lett.*, vol. 31, no. 20, pp. 2975–2977, Oct. 2006.
[41] J. P. Kolb, T. Pfeiffer, M. Eibl, H. Hakert, and R. Huber, "High-resolution retinal swept source optical coherence tomography with an ultra-wideband Fourier-domain mode-locked laser at MHz A-scan rates," *Biomed. Opt. Exp.*, vol. 9, no. 1, pp. 120–130, Jan. 2018.
[42] B. R. Biedermann, W. Wieser, C. M. Eigenwillig, T. Klein, and R. Huber, "Dispersion, coherence and noise of Fourier domain mode locked lasers," *Opt. Exp.*, vol. 17, no. 12, pp. 9947–9961, Jun. 2009.
[43] F. Yang, W. Zhang, S. Zhao, Q. Liu, J. Tao, and Z. He, "Miniature interrogator for multiplexed FBG strain sensors based on a thermally tunable microring resonator array," *Opt. Exp.*, vol. 27, no. 5, pp. 6037–6046, Mar. 2019.

Tatsuya Yamaguchi (Member, IEEE) received the B.S., M.S., and Ph.D. degrees in engineering from Nihon University, Tokyo, Japan, in 2013, 2015, and 2018, respectively. He joined the Department of Electrical Engineering, Nihon University. His current research interests include optical measurements, digital signal processing, structural health monitoring, and optical fiber sensing. He is a member of the Institute of Electrical Engineers of Japan (IEEJ) and the Society of Instrument and Control Engineers (SICE).

Wataru Endo (Member, IEEE) received the B.S. and M.S. degrees in engineering from Nihon University, Tokyo, Japan, in 2019 and 2021, respectively. He has been employed by Tokyo Metropolitan Government. His current research interest includes optical fiber sensing.

Yukitaka Shinoda (Member, IEEE) received the B.Sc., M.Sc., and Ph.D. degrees in electrical engineering from Nihon University in 1987, 1989, and 2004, respectively. He was a Visiting Researcher with the Virginia Polytechnic Institute and State University (Virginia Tech) from 2009 to 2010. Since 2012, he has been a Professor with the College of Science and Technology, Nihon University. He has focused on laser sensing, digital signal processing, motion analysis, and optical scanning holography. He is a member of the Institute of Electrical Engineers of Japan (IEEJ), the Society of Instrument and Control Engineers (SICE), the Japan Society of Applied Physics (JSAP), and the International Society for Optical Engineering (SPIE).